Journal of Rock Mechanics and Geotechnical Engineering 18 (2026) 3471–3482

Contents lists available at ScienceDirect

Journal of Rock Mechanics and Geotechnical Engineering

journal homepage: www.jrmge.cn

Full Length Article

Effect of confining pressures on the drilling parameters and specific energy: Insights into determining in situ stress using drilling monitoring techniques

Wendal Victor Yue [a], Manchao He [b], Hehua Zhu [a,*], Zhongwen Yue [b], Sichen Long [b], Mengjia Zhang [b]

[a] Department of Geotechnical Engineering, College of Civil Engineering, Tongji University, Shanghai, 200092, China
[b] School of Mechanics and Civil Engineering, China University of Mining and Technology (Beijing), Beijing, 100083, China

ARTICLE INFO

Article history:
Received 13 February 2025
Received in revised form
29 May 2025
Accepted 2 June 2025
Available online 3 September 2025

Keywords:
Drilling monitoring test
Drilling specific energy
In-situ stress determination
Confining stresses

ABSTRACT

Current in-situ stress determination methods are typically conducted inside a drillhole after its creation. However, the drilling process itself is not utilized for measuring in-situ stress or rock strength, despite being a form of direct mechanical testing on the rock mass. Crucially, drilling contains valuable information about in-situ stress and rock strength, as rocks under high compressive stresses exhibit greater strength. This paper presents a novel in-situ stress determination method, supported by the experimental result of rock drilling monitoring tests using a mine hydraulic-rotary drilling machine. Key drilling parameters-including thrust force, rotation speed, torque and drilling speed-are monitored in real time to determine the drilling specific energy per unit volume of rock. A concave-upward relationship between drilling specific energy and rotation speed is identified, which can characterize rock compressive strength and tensile strength with consistent regularity. Further drilling tests are conducted on the same rock samples under varying confining pressures. Results indicate that as confining pressure increases, the concave-upward curve of drilling specific energy shift upward, reflecting enhanced rock strengths due to confinement. The paper outlines the complete methodology for in-situ stress determination using drilling monitoring techniques, bridging the research gaps among drilling monitoring, rock mechanics, and in-situ stress analysis.

1. Introduction

In situ rock stress data are fundamental for understanding subsurface stress states and boundary conditions in geotechnical engineering analyses during design and construction phases (Hudson and Harrison, 1997). Current stress determination methods can be classified as indirect or direct approaches. Indirect methods include borehole breakout analysis (Han et al., 2020), core discing interpretation (Ishida and Saito, 1995), and acoustic emission (Kaiser effect) measurement (Seto et al., 1997). Direct methods include flatjack testing (Forbes et al., 2020), hydraulic fracturing (Haimson and Cornet, 2003) and overcoring techniques (Sjöberg et al., 2003; Li et al., 2025). Most of these methods require pre-existing drillholes to install sensors or equipment at target depths, relying on deformation characteristics around circular openings to estimate stress concentrations. However, they face significant limitations, including: depth restrictions, high operational costs, field implementation challenges and reliance on simplifying assumptions during stress back-calculation (Han et al., 2020; Lin et al., 2020; Mckenney and Corkum, 2020; Zou et al., 2021; Li et al., 2022, 2025; Neuner et al., 2023; Zhao and Qin, 2023).

Given that drilling is an essential prerequisite for most in situ stress determination methods, integrating drilling monitoring techniques during stress measurement campaigns presents a practical opportunity. This approach involves equipping drilling equipment with multi-sensor systems to record operational parameters in real-time, enabling simultaneous characterization of both geomechanical properties (e.g., rock strength) and structural features (e.g., bedding depth) during the drilling process (Yue

* Corresponding author.
E-mail address: zhuhehua@tongji.edu.cn (H. Zhu).

Peer review under responsibility of Institute of Rock and Soil Mechanics, Chinese Academy of Sciences.

https://doi.org/10.1016/j.jrmge.2025.06.026

et al., 2004, 2024; Chen and Yue, 2016; Wang et al., 2022; Wu et al., 2024a, 2024b, 2025).

The influence of in situ stresses on drilling response is typically investigated through controlled laboratory tests on confined rock samples. Researchers have employed various approaches: predefined bit-rock interaction model (Li et al., 2021; Ding et al., 2024; Zhao et al., 2024) and specific energy analysis using Teale's (1965) concept. Liu et al. (2023) and Tang et al. (2023) analysed the drilling specific energy for rock samples applied with different confining pressure conditions. While these studies utilized rectangular samples confined by four pressure platens (with open top/bottom faces for drilling), they notably omitted examination of specific energy development across varying drilling parameters (e.g., thrust force, rotation speed). This represents a critical gap in understanding the complete specific energy-drilling response relationship.

Previously, Yue et al. (2025) developed a novel model correlating drilling specific energy with rock strength parameters. The model utilizes the fundamental concept of specific energy, W_d, which is defined as the drilling work required to excavate a unit volume of rock (Teale, 1965). For non-percussive rotary drilling operations, the total specific energy (W_d, in J/m^3) is calculated as the sum of two distinct thrust energy W_t and rotary energy W_r components:

$$W_d = W_t + W_r \tag{1}$$

$$W_t = \frac{F_t v}{Av} \tag{2}$$

$$W_r = \frac{F_r v_r}{Av} = \frac{2T\pi rRPM}{Avr} = \frac{2\pi RPMT}{Av} \tag{3}$$

where F_t is the thrust force (N), v is the drilling speed (m/min), A is the cross-sectional area of drillhole (m^2), F_r is the rotational force (N) which is equal to T/r, T is the drilling torque (Nm), r is the drill bit radius (m), v_r is the rotational linear velocity (m/min), and RPM is the revolution per minute (r/min).

The equations above describe the energy expended or work done (W_d, in J/m^3) to produce one unit volume of drill hole with a cross-sectional area (A, in m^2). This energy is a function of the thrust force (F_t, in N) and the rotational speed (RPM, in r/min), which together generate a torque (T, in Nm) and a drilling speed (v, in m/min). The volume of rock removed per minute under these drilling conditions is the product of the cross-sectional area and the drilling rate, or Av (in m^3/min).

Drilling specific energy represents the mechanical work required to excavate a unit volume of rock, characterizing the energy input needed to fragment intact rock during drilling. This parameter is not constant but varies significantly with operational conditions, particularly thrust force, as first demonstrated by Teale (1965) through sandstone drilling tests revealing a characteristic concave-upward relationship. The pattern shows initially high energy consumption at low thrust forces, gradually decreasing to an optimal minimum before slightly rising again under excessive thrust, reflecting transitions from inefficient surface grinding to effective chip formation and eventually over-fragmentation. This fundamental relationship has been consistently validated across multiple studies (Teale, 1965; Hoberock and Bratcher, 1996; Rao et al., 2002; Yaşar et al., 2011; Feng et al., 2020; Sakız et al., 2021; Yu et al., 2021; Yue et al., 2025), establishing drilling specific energy's critical role in understanding rock fragmentation mechanics during drilling operations.

Yue et al. (2025) attributed the concave-upward relationship between drilling specific energy and thrust force to hybrid rock failure modes during drilling operations. Their findings suggest that high thrust forces promote compressive shear failure, while low thrust conditions favor tensile failure mechanisms. The use of drilling specific energy as a rock strength indicator (Hoberock and Bratcher, 1996; Gao et al., 2024) offers significant advantages, including straightforward calculation and reliance on real-time measurements of thrust force, rotation speed, torque, and drilling speed without requiring theoretical assumptions.

As a result, this study employs the drilling specific energy method to analyze results from controlled drilling tests conducted using a mine hydraulic-rotary drilling machine on rectangular rock prism samples subjected to varying confining pressures through steel plate compression via hydraulic jacks. The research objectives are threefold: (1) to develop a practical model correlating drilling specific energy with rock strength under confining pressure effects, (2) to investigate how confining pressure influences drilling parameters and specific energy, and (3) to establish a novel in situ stress determination method by systematically incorporating confining pressure effects into a drilling monitoring-based analytical framework.

2. Hydraulic rotary drilling test set up

2.1. Hydraulic rotary drilling machine and monitoring system

The drilling tests were conducted using a hydraulic-rotary drilling machine mounted on a two-boom, pilot-hydraulic controlled face drilling rig (Model CZMY2-105/25; Fig. 1), a system typically employed for rock bolt hole drilling in underground coal mines. The setup utilized drill bits equipped with twin PDC cutters capable of producing 28-mm-diameter boreholes. To minimize frictional interference during operation, 20-mm-diameter hollow drill rods were employed, which simultaneously served as conduits for water-based drilling fluid delivery from the pump system to the bit interface. This fluid circulation provided essential cooling and lubrication functions to mitigate bit wear effects. Consistent testing conditions were maintained by using a new drill bit for each experimental drillhole. The integrated monitoring system incorporated a pull-rope displacement sensor, hydraulic pressure sensors, and a torque-rotation speed sensor, enabling comprehensive time-series data acquisition. Thrust force values were derived from calibrated hydraulic pressure measurements, while drilling speed was calculated from displacement data records,

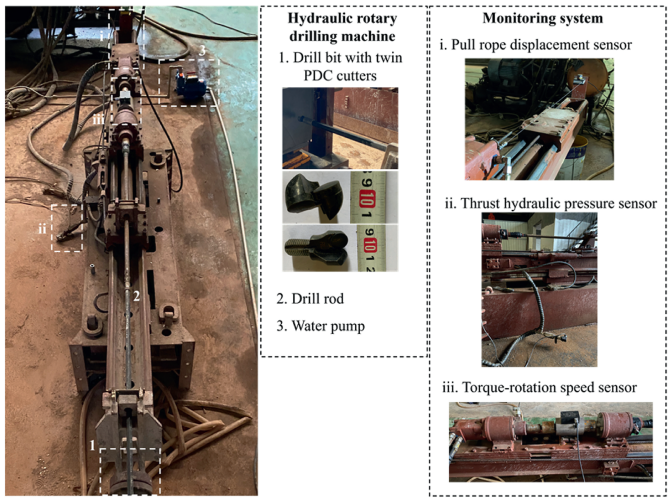

Fig. 1. Hydraulic rotary drilling machine and monitoring system.

with simultaneous monitoring of rotation speed and torque parameters throughout all test sequences.

2.2. Rock samples and mechanical properties

Three distinct sandstones (designated S1, S2, and S3) were cut into rectangular prism specimens for drilling tests. These sandstones, collected from different geological formations within China's Sichuan Province, exhibit varying strength characteristics and mechanical properties. Unconfined compression tests and splitting tensile tests were conducted in accordance with American Society for Testing and Materials (ASTM D7012-23, 2023; ASTM D3967-23, 2023). Table 1 presents the resulting unconfined compressive strength (UCS) and tensile strength values for each sample, representing averages of five and ten tests for compressive and tensile strength measurements, respectively.

2.3. Confining pressure loading platform

A custom loading platform was designed to apply controlled confining pressure during drilling tests (Fig. 2). The system generates biaxial compression through two hydraulic jacks that apply orthogonal stresses to the rock sample, simulating in situ principal stress conditions. Steel pressure platens uniformly distribute stresses across all sample surfaces. Integrated load cells positioned between the jacks and platens provide real-time measurement of both vertical and horizontal pressures. Due to system limitations, the maximum achievable confining stress is 1 MPa.

2.4. Summary of test series

Table 2 shows the summary of all tests conducted in this study. Three different sandstones are drilled under rotation speeds of 200 r/min, 250 r/min and 300 r/min. Under each rotation speed condition, three levels of confining stress are selected: 0 MPa (without confining pressure), 0.5 MPa and 1 MPa. This study employs an equi-biaxial loading condition (identical vertical and horizontal stresses) following established experimental protocols (Li et al., 2021; Ru et al., 2022; Liu et al., 2023; Tang et al., 2023). The symmetrical stress configuration was specifically selected to isolate and evaluate the fundamental relationship between confining stress and drilling-specific energy response, which represents the primary objective of this investigation. While this approach effectively demonstrates the confinement effect on rock strength characterization, future research will address more complex stress states involving principal stress magnitude variations and orientation effects to expand the method's field applicability.

All tests were conducted with a standardized drilling distance of 300 mm, with real-time drilling parameters recorded at a sampling frequency of 7 Hz. Prior to the main test series, repeated trials under identical drilling conditions were performed to verify measurement precision. While no formal standards currently exist for rock drilling monitoring tests, empirical evidence suggests that constant penetration rates and stable drilling parameters are achievable when operating in homogeneous rock under consistent drilling conditions. The selected 300 mm drilling distance for the 28 mm diameter bit (a drilling distance to bit diameter ratio of 10.7) was determined based on extensive experimental validation (Yue et al., 2023; Long et al., 2025; Yue et al., 2025), which confirmed that this configuration reliably produces representative, steady-state drilling responses. This distance ensures sufficient rock interaction to obtain meaningful averages of drilling speed and other parameters while minimizing boundary effects. For smaller samples or shorter drilling distances where full stabilization cannot be achieved, repeated testing is recommended to obtain statistically reliable results.

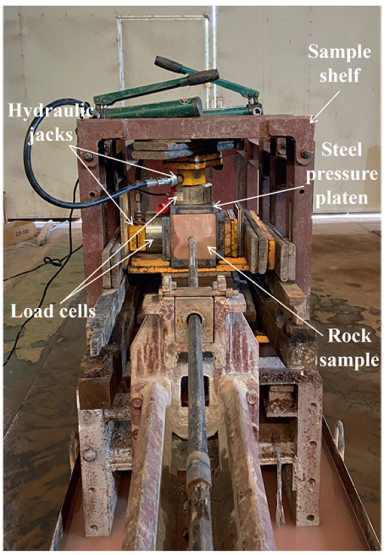

Fig. 2. Confining pressure loading platform.

Table 2
Test conditions.

Rock ID	Test conditions	
	Confining stress (MPa)	Rotation speed (r/min)
S1/S2/S3	0	200
		250
		300
	0.5	200
		250
		300
	1	200
		250
		300

3. Results analysis of the drilling specific energy model for drilling tests without confining pressure

3.1. Result of drilling tests without confining pressure

The initial phase of this study examines the effect of rock strength on drilling parameters. Drilling tests were conducted on

Table 1
Strength of three different sandstones used in this study.

Rock type	Sample ID	Unconfined compressive strength (MPa)	Tensile strength (MPa)
Sandstone	S1	9.49	1.19
	S2	14.56	1.75
	S3	35.88	3.81

the three sandstone samples without confining pressure. Each sample was clamped and secured on the sample shelf. The drilling machine's manual rotation speed control enabled testing at three specified speeds: 200 r/min, 250 r/min, and 300 r/min.

Fig. 3 presents complete time-series drilling results for S1, S2, and S3 at 200 r/min. The displacement data exhibits a strong linear relationship with time, allowing fitting of a linear regression line. *Following* Yue et al. (2025)*, the regression slope represents the average drilling speed. The rotation speed remained stable at the target 200* r/min *throughout all tests.*

Both thrust force and torque demonstrate similar behavioral patterns. At drilling initiation, these parameters rapidly peak before slightly decreasing and stabilizing at near-constant values for the test duration. The average values from this stable phase are used for subsequent analyses.

Complete time-series results for 250 r/min and 300 r/min tests are presented in the Appendix *(*Fig. A1 and A2*).*

3.2. Summary of drilling parameters without confining pressure

The consistency of drilling parameters has been a major challenge in drilling monitoring studies (Deng et al., 2022; Ma et al., 2022; Dai et al., 2024). Fig. 4 plots the average thrust force, torque, and drilling speed for the three sandstones against their rotational speed.

A practical way to describe drilling parameters is to treat thrust force and rotational speed as control parameters (independent variables), while torque and drilling speed act as response parameters (dependent variables) that depend on both the control parameters and rock strength.

Thrust force refers to the axial force applied by the drill bit onto the rock. Theoretically, thrust force is linearly proportional to torque based on the principles of normal and shear forces. However, drilling differs from static mechanical tests because it involves dynamic motion (i.e., the drill bit advances into the rock).

A lower-strength rock typically results in lower torque (as seen in Fig. 4b) and higher drilling speed. While Fig. 4c does not fully align with the theoretical expectation—where lower strength should consistently yield higher drilling speed—this discrepancy arises due to variations in the applied thrust force.

If rocks are drilled under identical thrust force and rotational speed conditions, the anticipated trends are low-strength rock would result in a lower torque and a higher drilling speed. While high-strength rock would result in a higher torque and a lower drilling speed. In this ideal scenario, drilling speed could serve as an indicator of rock strength.

However, the key finding of this study is that rock strength cannot be reliably characterized by a single drilling parameter alone. Instead, it is recommended to evaluate drilling performance using drilling specific energy, as it provides a comprehensive mechanical description of the drilling process by incorporating all relevant parameters (including drillhole dimensions) based on Newtonian mechanics.

3.3. Drilling specific energy model for rock strength characterization

Drilling-specific energy W_d represents the work required to drill a unit volume of rock under specific conditions of thrust force, rotational speed, torque, and drilling speed. It serves as an indicator of rock strength (Teale, 1965; Yue et al., 2025). Under identical thrust force and rotational speed, higher-strength rocks yield higher W_d values, meaning they require more energy to drill.

Table 3 summarizes the drilling-specific energy values

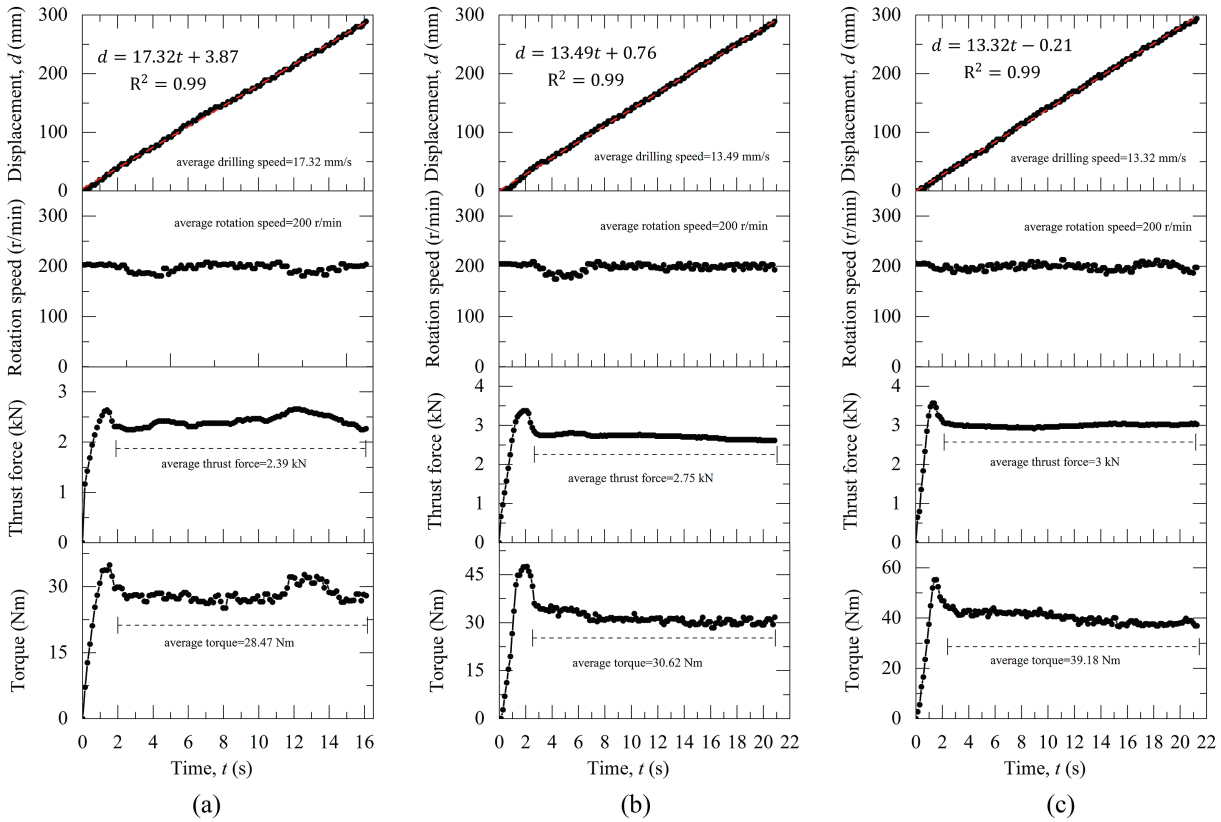

Fig. 3. Time series drilling results with rotation speed 200 r/min: (a) S1, (b) S2, and (c) S3.

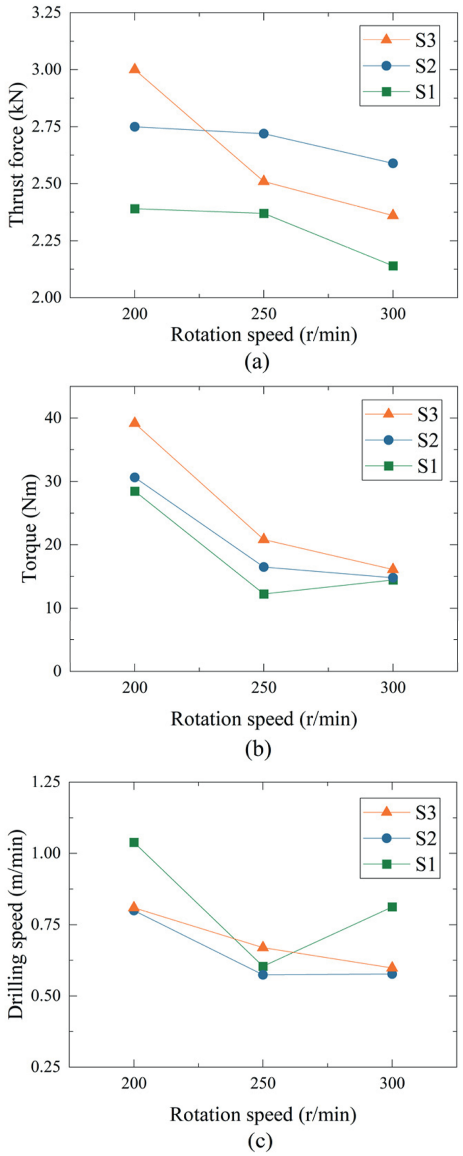

Fig. 4. Change of drilling parameters with respect to its rotation speed: (a) Thrust force, (b) Torque, and (c) Drilling speed.

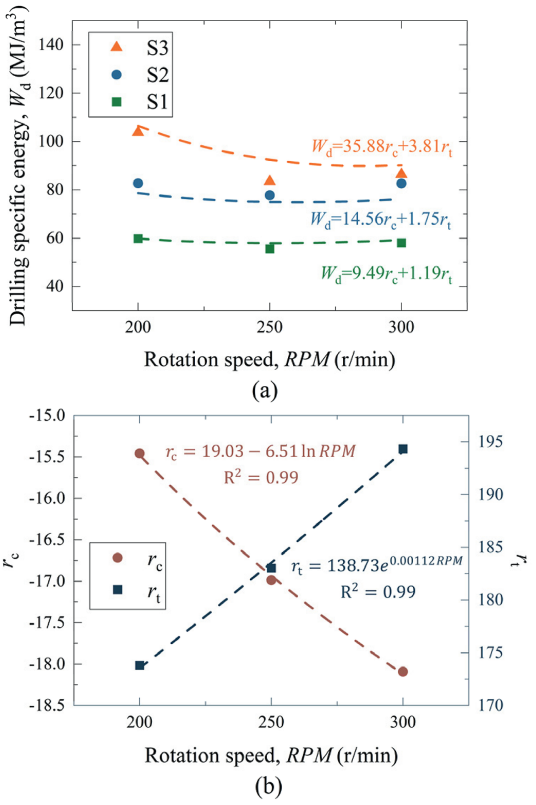

Fig. 5. Drilling specific energy model for rock strength characterization: (a) Drilling specific energy with respect to rotation speed, and (b) Empirical regression functions of r_c and r_t with rotation speed.

calculated from drilling parameters (thrust force, rotational speed, torque, and drilling speed) using Eqs. (1)–(3) for a 28 mm diameter drillhole. Fig. 5a plots W_d against rotational speed for the three sandstones, revealing a concave-upward trend. Generally, a higher curve position corresponds to greater rock strength, consistent with prior studies (Teale, 1965; Hoberock and Bratcher, 1996; Rao et al., 2002; Yaşar et al., 2011; Feng et al., 2020; Sakız et al., 2021; Yu et al., 2021; Yue et al., 2025).

Since the drilling tests were conducted on unconfined samples, the drilling specific energy W_d can be correlated with both the uniaxial compressive strength σ_c and tensile strength σ_t, as determined by uniaxial compression tests and Brazilian splitting tests (Table 1):

$$W_d = r_c\sigma_c + r_t\sigma_t \tag{4}$$

where r_c and r_t are empirical coefficients determined by multivariate regression. For each rotational speed, the drilling specific energy W_d of the three sandstones (S1, S2, and S3) can be expressed in terms of their corresponding uniaxial compressive strength σ_c and tensile strength σ_t as follows:

Table 3
Summary of thrust force, torque, drilling speed and drilling specific energy W_d for drilling tests without confining pressure at different rotation speeds.

Sample ID	Rotation speed (r/min)	Thrust force (kN)	Torque (Nm)	Drilling speed (m/min)	W_d (MJ/m^3)
S1	200	2.39	28.47	1.04	59.79
	250	2.37	12.25	0.60	55.62
	300	2.14	14.47	0.81	58.00
S2	200	2.75	30.62	0.80	82.66
	250	2.72	16.49	0.57	77.75
	300	2.59	14.79	0.58	82.65
S3	200	3	39.18	0.81	103.66
	250	2.51	20.81	0.67	83.43
	300	2.36	16.12	0.60	86.33

$$\begin{bmatrix} W_{d,S1} \\ W_{d,S2} \\ W_{d,S3} \end{bmatrix} = r_c \begin{bmatrix} \sigma_{c,S1} \\ \sigma_{c,S2} \\ \sigma_{c,S3} \end{bmatrix} + r_t \begin{bmatrix} \sigma_{t,S1} \\ \sigma_{t,S2} \\ \sigma_{t,S3} \end{bmatrix} \quad (5)$$

As a result, three pairs of r_c and r_t values were obtained at three different rotational speed levels (200 r/min, 250 r/min, and 300 r/min). These r_c and r_t values are plotted against their corresponding rotational speeds in Fig. 5b. Furthermore, the results indicate that both r_c and r_t values exhibit a dependence on rotational speed, suggesting that empirical functions could be developed to describe these relationships:

$$r_c = 19.03 - 6.51 \ln RPM \quad (6)$$

$$r_t = 138.73 e^{0.00112 RPM} \quad (7)$$

Another key observation reveals an inverse relationship between rotational speed and the empirical coefficients: as rotational speed increases, r_c decreases while r_t increases. This trend shows that tensile strength becomes the dominant factor in rock drilling at higher rotational speeds. These findings suggest that the drilling process represents a hybrid failure mechanism, transitioning from compressive-shear dominated failure to extension-dominated failure as rotational speed increases.

Based on Eqs. (4)–(7), a comprehensive empirical equation can be developed to characterize drilling specific energy W_d (MJ/m^3) that incorporates compressive shear strength σ_c (MPa), tensile strength σ_t (MPa) and rotation speed RPM (r/min). The general form of this equation is as follows:

$$W_d = (19.03 - 6.51 \ln RPM)\sigma_c + \left(138.73 e^{0.00112 RPM}\right)\sigma_t \quad (8)$$

The three dashed lines in Fig. 5a were determined by substituting the compressive strength σ_c and tensile strength σ_t values for each sandstone into Eq. (8) across the rotational speed range of 200–300 r/min. The close alignment between these dashed lines and the experimental data confirms the reliability of Eq. (8).

4. Results analyses of drilling specific energy model for drilling tests with confining pressure

4.1. Result of drilling tests with confining pressures

As described in Section 2.3, the confining platform can apply a maximum confining stress σ_p of 1 MPa to the sample. To simplify the analysis at this stage, equal confining pressures were applied in both vertical and horizontal directions. Three confining stress levels were selected: 0 MPa, 0.5 MPa, and 1 MPa. For each stress level, three drillholes were made in each sandstone sample at rotational speeds of 200 r/min, 250 r/min, and 300 r/min.

Fig. 6 shows the time-series drilling results under different confining pressures at a constant rotational speed of 250 r/min. While the confining pressures clearly influence the drilling results, the overall data patterns remain consistent. The displacement data shows a linear relationship with time, allowing the average drilling speed to be determined from the slope of the linear regression line. Although minor fluctuations occur, the rotational speed remains stable at the target 250 r/min level. Both thrust force and torque follow similar patterns, rapidly peaking when drilling begins before gradually stabilizing at constant values until test completion. This demonstrates the close relationship between thrust force and torque. When the drill bit contacts the rock surface, frictional resistance generates dynamic torque, resulting in angular acceleration of the drill bit.

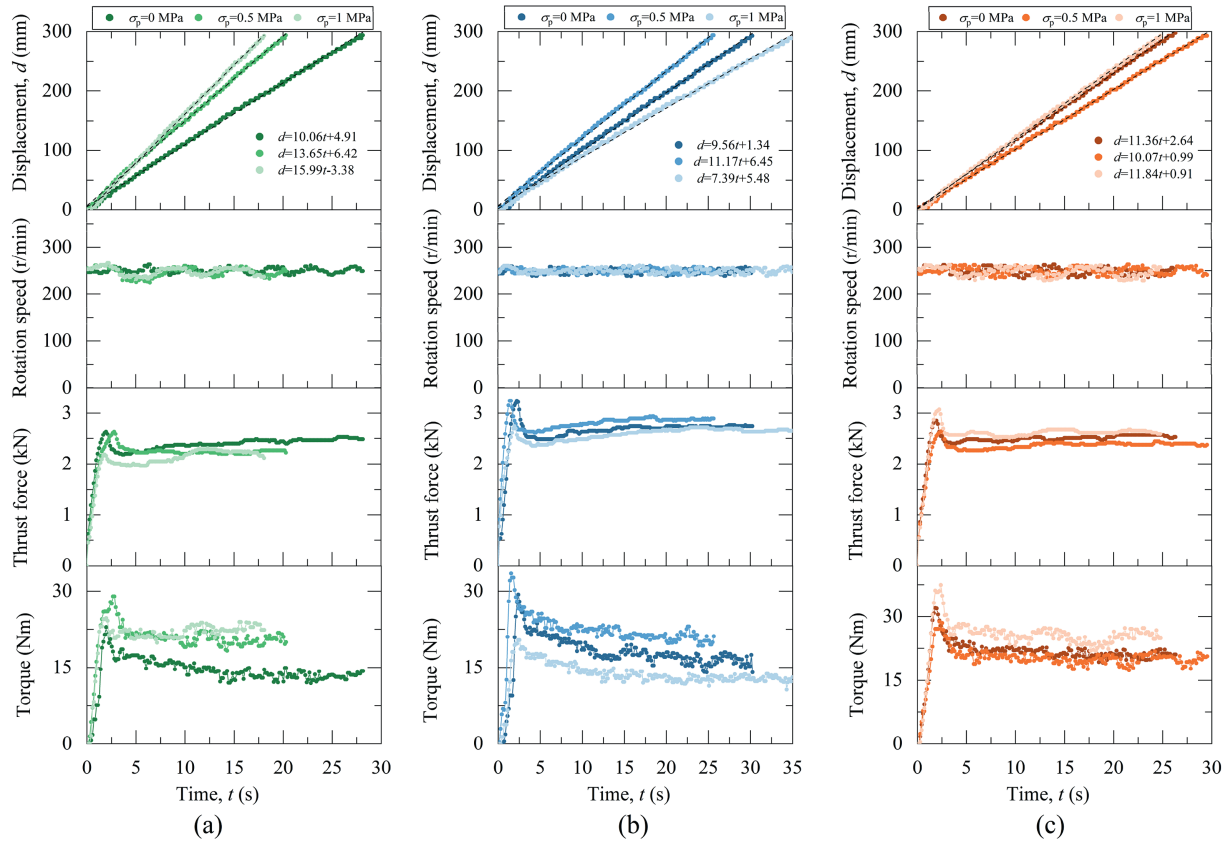

Fig. 6. Time series drilling results with three confining pressures at the rotation speed of 250 r/min: (a) S1, (b) S2, and (c) S3.

The corresponding time-series drilling results for 200 r/min and 300 r/min under confining pressures are provided in the Appendix (Fig. A3 and A4).

4.2. Effect of confining pressures on drilling parameters and drilling specific energy

Fig. 7 summarizes the drilling parameters and drilling specific energy results under different confining pressures, with complete data presented in Table 4.

The results demonstrate a general proportionality between thrust force and torque. However, developing either analytical or empirical equations to quantify the effect of confining pressures on thrust force, torque, and drilling speed remains challenging. For future drilling parameter analysis, we recommend investigating torque, drilling speed, and drilling specific energy behavior under controlled thrust force and rotational speed conditions.

The regularity of drilling specific energy is evident in Fig. 7d, h, and 7l for S1, S2, and S3 sandstones, respectively. All results exhibit a concave-upward trend in the relationship between W_d and rotational speed. Notably, increasing confining pressure elevates the entire concave-upward curve, indicating greater energy requirements. This observation aligns with the well-established principle that rock strength increases under confinement.

Furthermore, the results clearly show that drilling-specific energy is not constant but rather follows this consistent concave-upward pattern with rotational speed. This phenomenon helps explain the discrepancies between the findings of Liu et al. (2023) and Tang et al. (2023). These findings strongly support applying the drilling-specific energy model (Section 3.3) to analyze rock strength variations under confining pressures.

4.3. Interpretating rock strengths under confining pressures from drilling specific energy model

4.3.1. Solving σ_c and σ_t using Cramer's rule

Based on Eq. (8), which incorporates the pre-determined drilling specific energy model, interpreting rock strength parameters (σ_c and σ_t) essentially involves solving a system of equations with two variables. A solution method based on Cramer's Rule is introduced, as this approach can be readily implemented in Excel spreadsheets or other computer programs to enable rapid, automated calculations.

Consider two drillholes performed on the same rock under identical confining pressure conditions but with different rotational speeds (RPM_1 and RPM_2):

$$r_{c1}\sigma_c + r_{t1}\sigma_t = W_{d1} \tag{9}$$

$$r_{c2}\sigma_c + r_{t2}\sigma_t = W_{d2} \tag{10}$$

The coefficients r_{c1} and r_{t1} are calculated using Eqs. (6) and (7), respectively, with RPM_1, while r_{c2} and r_{t2} are determined using RPM_2. A key assumption of this approach is that the functional dependence of r_c and r_t on rotational speed (as described by Eqs. (6) and (7)) remains unaffected by confining stress. W_{d1} and W_{d2} represent the drilling-specific energy values computed from the monitored drilling data for RPM_1 and RPM_2, respectively, using Eqs. (1)–(3).

The compressive strength σ_c and tensile strength σ_t of the drilled rock can then be determined as follows:

$$\sigma_c = \frac{D_x}{D} \tag{11}$$

$$\sigma_t = \frac{D_y}{D} \tag{12}$$

And the variables D, D_x and D_y can be determined as follows:

$$D = \begin{vmatrix} r_{c1} & r_{t1} \\ r_{c2} & r_{t2} \end{vmatrix} \tag{13}$$

$$D_x = \begin{vmatrix} W_{d1} & r_{t1} \\ W_{d2} & r_{t2} \end{vmatrix} \tag{14}$$

$$D_y = \begin{vmatrix} r_{c1} & W_{d1} \\ r_{c2} & W_{d2} \end{vmatrix} \tag{15}$$

A quick check can be conducted if D is non-zero value, indicating the system has a unique solution. In contrast, if D is zero, the system has either no solution or infinitely many solutions.

4.3.2. Effect of confining pressures on σ_c and σ_t

Table 5 presents the compressive strength σ_c and tensile strength σ_t for S1, S2, and S3 sandstones derived from drilling tests under various confining pressures. The results show that σ_c and σ_t values obtained from unconfined drilling tests ($\sigma_p = 0$) agree well with those determined from conventional mechanical tests (unconfined compression tests and Brazilian splitting tests).

Fig. 8 plots the relationship between σ_c and σ_t and their corresponding confining pressure σ_p. The data indicate that both strength parameters increase slightly with confining pressure within the 0–1 MPa range. The following linear regression form of Eqs. (16) and (17) are recommended:

$$\sigma_c = m_1 - m_2 \times m_3{}^{\sigma_p} \tag{16}$$

$$\sigma_t = n_1 - n_2 \times n_3{}^{\sigma_p} \tag{17}$$

And the σ_c and σ_t at no confining pressures are denoted as $\sigma_{c,0}$ and $\sigma_{t,0}$ respectively:

$$\sigma_{c,0} = m_1 - m_2 \tag{18}$$

$$\sigma_{t,0} = n_1 - n_2 \tag{19}$$

Further research is required to determine whether the σ_c and σ_t derived from drilling tests using the proposed drilling specific energy model can accurately represent rock strengths measured through conventional triaxial testing methods, including triaxial compression tests (Hoek and Brown, 2019) and triaxial tensile tests (Ramsey and Chester, 2004). It is well established that rock compressive strength increases with confining pressure, while experimental evidence demonstrates more complex behavior for tensile strength under confinement. Under low confining pressures (<5 MPa), tensile strength typically shows an initial increase. Ma et al. (2024) observed this phenomenon in granite through multi-fracturing tests, reporting that tensile strength rises to a peak value at 2–5 MPa before gradually decreasing at higher pressures. Similarly, Liu et al. (2024) demonstrated a nonlinear increase in the dynamic tensile strength of sandstone under lateral confinement up to 15 MPa using dynamic split tests conducted with a triaxial Hopkinson bar (TriHB) system.

4.3.3. Developing a general drilling specific energy model

Fig. 9 displays both the measured drilling specific energy values (W_d, shown as markers) and the corresponding regression curves obtained by substituting the calculated σ_c and σ_t values at different confining pressures into Eq. (8).

In Fig. 9, the sandstone samples are color-coded as follows:

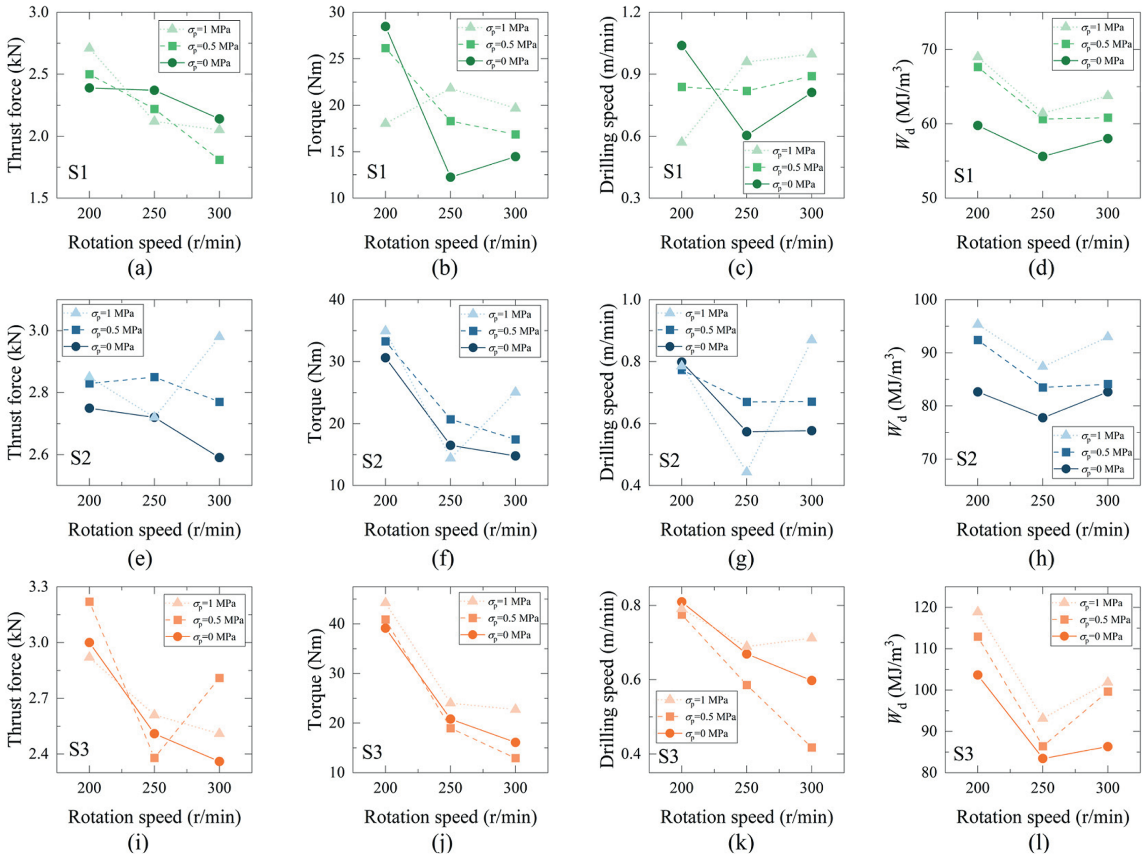

Fig. 7. Summary of drilling parameters result with different confining pressures: (a) S1 thrust force, (b) S1 torque, (c) S1 drilling speed, (d) S1 drilling specific energy, (e) S2 thrust force, (f) S2 torque, (g) S2 drilling speed, (h) S2 drilling specific energy, (i) S3 thrust force, (j) S3 torque, (k) S3 drilling speed, and (l) S3 drilling specific energy.

Table 4
Summary of drilling parameters and drilling specific energy W_d at different confining stresses σ_p for S1, S2 and S3 sandstones.

Sample ID	σ_p (MPa)	Rotation speed (r/min)	Thrust force (kN)	Torque (Nm)	Drilling speed (m/min)	W_d (MJ/m^3)
S1	0	200	2.39	28.47	1.04	59.79
		250	2.37	12.25	0.60	55.62
		300	2.14	14.47	0.81	58.00
	0.5	200	2.5	26.14	0.84	67.66
		250	2.22	18.31	0.82	60.64
		300	1.81	16.86	0.89	60.83
	1	200	2.71	18.02	0.57	68.99
		250	2.12	21.81	0.96	61.44
		300	2.05	19.68	1.00	63.78
S2	0	200	2.75	30.62	0.80	82.66
		250	2.72	16.49	0.57	77.75
		300	2.59	14.79	0.58	82.65
	0.5	200	2.83	33.28	0.77	92.41
		250	2.85	20.71	0.67	83.46
		300	2.77	17.45	0.67	84.13
	1	200	2.85	34.93	0.79	95.32
		250	2.72	14.42	0.44	87.38
		300	2.98	25.05	0.87	92.98
S3	0	200	3	39.18	0.81	103.66
		250	2.51	20.81	0.67	83.43
		300	2.36	16.12	0.60	86.33
	0.5	200	3.22	40.92	0.78	112.96
		250	2.38	18.97	0.59	86.42
		300	2.81	12.97	0.42	99.64
	1	200	2.92	44.24	0.79	118.91
		250	2.61	24.03	0.69	93.16
		300	2.51	22.75	0.71	101.86

Table 5
Summary of σ_c and σ_t with different confining pressures.

Items	σ_p (MPa)	σ_c (MPa)			σ_t (MPa)		
		S1	S2	S3	S1	S2	S3
Mechanical tests	0	9.49	14.56	35.88	1.19	1.75	3.81
Drilling tests	0	9.48	14.67	41.66	1.18	1.78	4.31
	0.5	17.79	22.89	45.94	1.97	2.57	4.74
	1	18.54	23.90	48.29	2.05	2.68	4.99

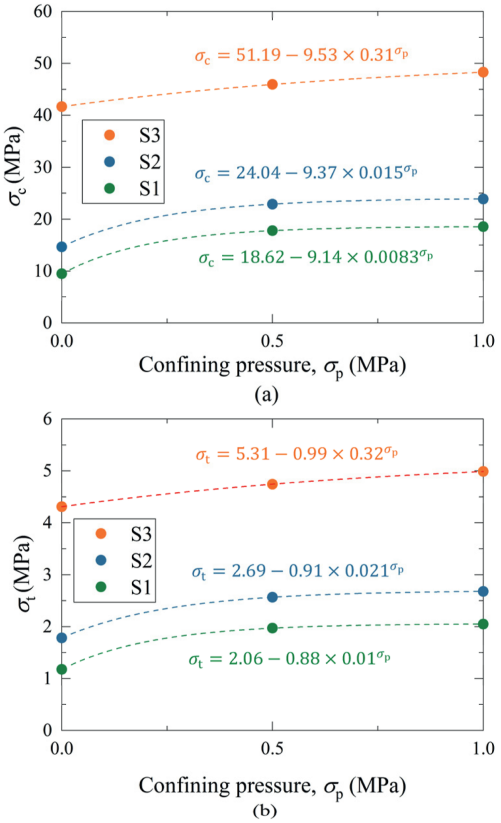

Fig. 8. σ_c and σ_t from drilling tests with corresponding σ_p: (a) σ_c and (b) σ_t.

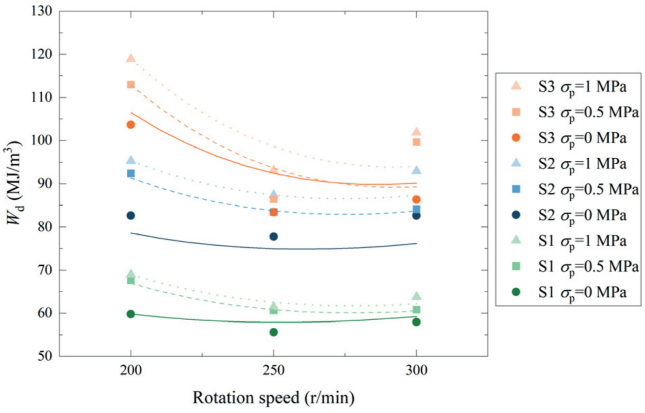

Fig. 9. Measured W_d (markers) and regression curves by substituting the calculated σ_c and σ_t at various confining pressures in Eq. (5).

green for S1, blue for S2, and orange for S3. The marker shapes indicate confining pressure conditions: dots represent $\sigma_p = 0$ MPa, squares represent $\sigma_p = 0.5$ MPa, and triangles represent $\sigma_p = 1$ MPa. The corresponding regression equations are provided in Table 6.

Table 6
Regression equations in Fig. 9 by substituting the calculated σ_c and σ_t at various confining pressures into Eq. (8).

ID	σ_p (MPa)	Regression equations for curves in Fig. 9
S1	0	$W_{d,S1,0} = 9.48r_c + 1.18r_t$
	0.5	$W_{d,S1,0.5} = 17.79r_c + 1.97r_t$
	1	$W_{d,S1,1} = 18.54r_c + 2.05r_t$
S2	0	$W_{d,S2,0} = 14.67r_c + 1.78r_t$
	0.5	$W_{d,S2,0.5} = 22.89r_c + 2.57r_t$
	1	$W_{d,S2,1} = 23.9r_c + 2.68r_t$
S3	0	$W_{d,S3,0} = 41.66r_c + 4.31r_t$
	0.5	$W_{d,S3,0.5} = 45.94r_c + 4.74r_t$
	1	$W_{d,S3,1} = 48.29r_c + 4.99r_t$

The regression curves follow distinct line styles: solid curves represent σ_c and σ_t at $\sigma_p = 0$ MPa, dashed curves correspond to $\sigma_p = 0.5$ MPa, and dotted curves show $\sigma_p = 1$ MPa. All regression curves display a concave-upward trend that aligns well with the experimentally measured drilling-specific energy values.

The model demonstrates satisfactory agreement with the actual drilling data. However, the accuracy could be further enhanced by expanding the dataset to refine the r_c and r_t functions (Eqs. (6) and (7)) through additional drilling tests on rocks with varying strength properties.

5. Potential in situ stress determination method using drilling monitoring technique

The complete sequence of the proposed in situ stress determination method using drilling monitoring techniques requires careful consideration. Fig. 10 presents a flow chart summarizing the three-phase methodology: (1) in situ drilling tests, (2) laboratory drilling tests, and (3) back analysis.

The first phase involves conducting in situ drilling while monitoring drilling parameters. For this purpose, Drilling Process Monitoring (DPM), originally developed by Yue et al. (2004), serves as a reliable and well-established technique. The acquired drilling data should be processed using time series analysis methods before interpretation, detail applications can refer to studies by Wang et al. (2021) and Wu et al. (2024b). Notably, the DPM technique is not constrained by drillhole length. Fig. 10 illustrates the application of an advanced hydraulic core drilling rig for tunnel face advancement, as tunnel in situ stresses are particularly relevant for geotechnical design. The DPM method is recommended for its ability to accurately capture critical drilling parameters, including thrust force, rotational speed, torque, and drilling speed.

In the second phase, retrieved rock cores undergo laboratory testing. These cores should be cut into rectangular prisms for compatibility with true triaxial testing systems (He et al., 2012), enabling simulation of high-confining stress conditions. However, system modifications are necessary to incorporate a drainage system and ensure waterproofing for wet drilling conditions. Sample size reduction during preparation may be addressed by using proportionally smaller drill bits with appropriate correction factors to account for size effects. This enhanced true triaxial system would facilitate a comprehensive investigation of principal stress magnitude and orientation effects on drilling monitoring results, ultimately refining the in situ stress determination methodology.

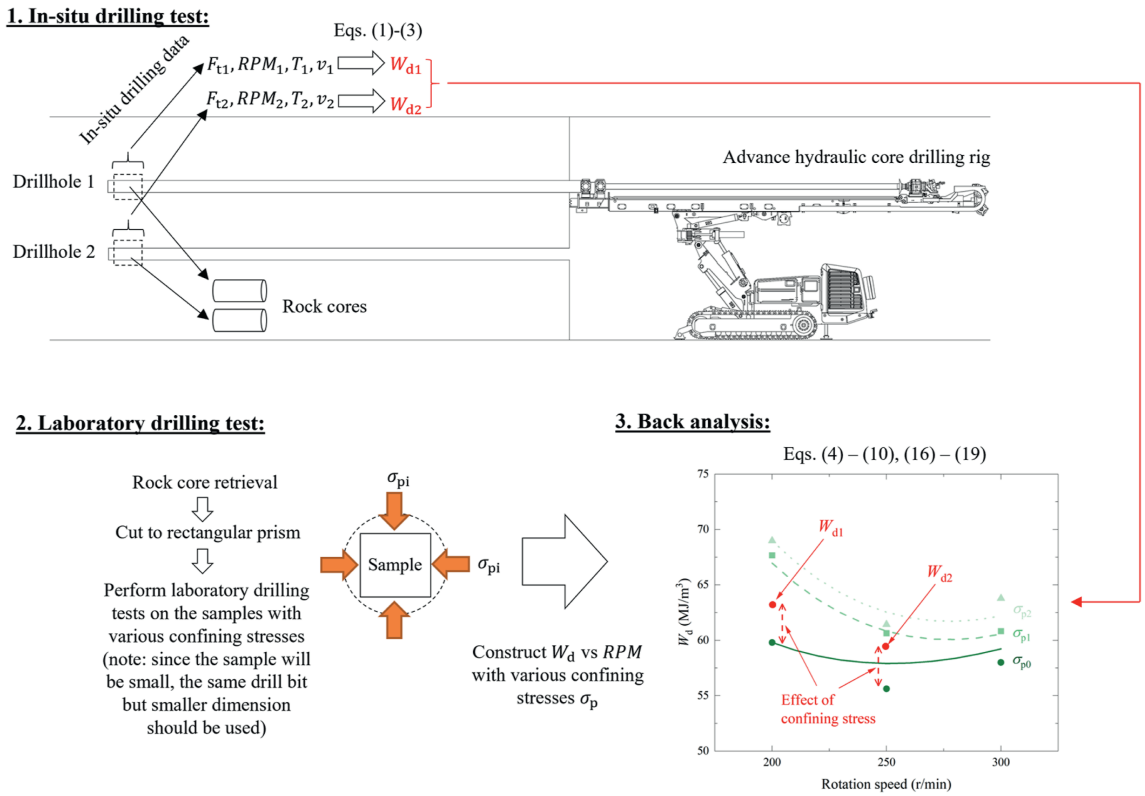

Fig. 10. Flow chart for the application of using drilling monitoring technique as an in situ stress determination method.

The final back analysis phase integrates laboratory and field data. Results from core drilling tests are used to establish W_d vs *RPM* relationships under various confining stresses (Section 4). In situ drilling measurements W_{d1} and W_{d2} are then superimposed on this model. These field-derived W_d values are expected to exceed laboratory measurements from unconfined conditions due to in situ stress effects.

This drilling monitoring approach offers distinct advantages over conventional methods as a direct measurement technique. It eliminates reliance on unverified assumptions, thereby reducing estimation uncertainties. The method is depth-independent, applicable to both shallow and deep measurements, and technically straightforward to implement using standard transducers. Many modern drilling rigs already incorporate the necessary monitoring systems, further simplifying adoption. Compared to existing techniques, this method provides a cost-effective, user-friendly solution with robust measurement capabilities across various depth ranges.

6. Conclusions

Despite its potential, drilling monitoring has not yet been established as a standard geotechnical testing method due to the absence of a robust theoretical framework for deriving rock mechanical properties from drilling data. This study addresses this critical gap by developing a novel drilling specific energy model that enables quantitative rock strength evaluation directly from drilling parameters. Furthermore, the proposed methodology demonstrates potential for extension to in situ stress determination, offering a promising alternative to conventional techniques. The key findings of this research include:

A novel model that characterizes both compressive and tensile rock strength through drilling specific energy analysis is presented. The model processes real-time drilling parameters, including thrust force, rotation speed, torque, and penetration rate - to quantify specific energy, which exhibits a distinctive concave-upward relationship with rotation speed. This characteristic curve serves as a diagnostic indicator of rock strength, with higher-strength rocks demonstrating proportionally elevated curve positions compared to weaker formations.

A systematic relationship between the concave-upward drilling-specific energy curve and confining stress is revealed. The results demonstrate that increasing confining stress produces an upward shift in the characteristic curve, providing direct quantitative evidence of confinement-induced rock strengthening. This consistent pattern establishes the curve's diagnostic value for evaluating in situ stress conditions.

Building upon these observed regularities, a novel in situ stress determination methodology based on drilling monitoring technology is introduced. The complete operational framework of this innovative approach is presented, including: (i) real-time acquisition and processing of drilling parameters, (ii) specific energy curve characterization under varying conditions, and (iii) quantitative stress evaluation through established correlation models. The method's implementation protocol, validation procedures, and potential field applications are systematically examined to demonstrate its practical viability for geotechnical assessments.

The proposed drilling-specific energy model demonstrates promising accuracy in estimating both rock strength parameters and confining stress magnitudes. While this represents a significant advancement for practical field applications, two important limitations warrant further investigation: (1) the current methodology does not determine principal stress orientations, which could potentially be addressed through integration with established techniques such as borehole image analysis or breakout interpretation; and (2) the effects of bit wear and dimensional

variations on model performance require systematic evaluation. Future research directions will focus on these critical aspects to enhance the model's comprehensive stress characterization capabilities and operational robustness.

CRediT authorship contribution statement

Wendal Victor Yue: Writing – original draft, Methodology, Formal analysis, Conceptualization, Writing – review & editing, Resources, Investigation, Data curation. **Manchao He:** Formal analysis, Conceptualization, Funding acquisition, Data curation. **Hehua Zhu:** Formal analysis, Conceptualization, Funding acquisition, Data curation. **Zhongwen Yue:** Formal analysis, Conceptualization, Funding acquisition, Data curation. **Sichen Long:** Investigation, Methodology, Conceptualization. **Mengjia Zhang:** Methodology, Conceptualization, Investigation.

Declaration of competing interest

The authors declare that they have no known competing financial interests or personal relationships that could have appeared to influence the work reported in this paper.

Acknowledgments

This study was supported by the National Natural Science Foundation of China (Grant Nos. 42272338 and 41902275). The first author thanks Chinese Government Scholarship for his PhD studies at Tongji University.

Appendix A. Supplementary data

Supplementary data to this article can be found online at https://doi.org/10.1016/j.jrmge.2025.06.026.

Abbreviations and symbols

A	Cross-sectional area of drillhole (m^2)
F_t	Thrust force (N)
F_r	Rotational force (N)
RPM	Revolution per minute (r/min)
r_c	Empirical coefficients for compressive strength
r_t	Empirical coefficients for tensile strength
T	Drilling torque (Nm)
v	Drilling speed (m/min)
v_r	Rotational linear velocity (m/min)
W_d	Drilling specific energy (J/m^3)
W_r	Drilling rotary energy (J/m^3)
W_t	Drilling thrust energy (J/m^3)
σ_c	Compressive strength (MPa)
σ_p	Confining stress (MPa)
σ_t	Tensile strength (MPa)

References

ASTM D3967-23, 2023. Standard Test Method for Splitting Tensile Strength of Intact Rock Core Specimens with Flat Loading Platens. ASTM International, West conshohocken, PA, USA.

ASTM D7012-23, 2023. Standard Test Methods for Compressive Strength and Elastic Moduli of Intact Rock Core Specimens Under Varying States of Stress and Temperatures. ASTM International, West conshohocken, PA, USA.

Chen, J., Yue, Z.Q., 2016. Weak zone characterization using full drilling analysis of rotary-percussive instrumented drilling. Int. J. Rock Mech. Min. 89, 227–234.

Dai, L., Li, S., Chen, Y., Li, P., Li, C., Zhang, H., Wang, Z., 2024. Thrust force prediction model coupled with the influence of material strain rate induced by cutting speed in CFRP drilling. J. Manuf. Process. 131, 1594–1610.

Deng, L.C., Li, X.Z., Xu, W., Xiong, Z., Wang, J., Qiao, L., 2022. Measurement while core drilling based on a small-scale drilling platform: mechanical and energy analysis. Measurement 204, 112082.

Ding, M., He, M., Yuan, Z., Wang, H., Luo, B., Ma, X., 2024. Application of the drilling mechanical properties of rock to determine confining pressure in shallow geological formations. Phys. Chem. Earth 135, 103650.

Feng, S., Wang, Y., Zhang, G., Zhao, Y., Wang, S., Cao, R., Xiao, E., 2020. Estimation of optimal drilling efficiency and rock strength by using controllable drilling parameters in rotary non-percussive drilling. J. Pet. Sci. Eng. 193, 107376.

Forbes, B., Vlachopoulos, N., Diederichs, M.S., Hyett, A.J., Punkkinen, A., 2020. An in situ monitoring campaign of a hard rock pillar at great depth within a Canadian mine. J. Rock Mech. Geotech. Eng. 12, 427–448.

Gao, H., Jiang, B., Ma, F., Wang, Q., Cai, S., Zhai, D., Wu, W., 2024. Detection methods for strength deterioration and structural characteristics of fractured rock based on digital drilling. Measurement 233, 114779.

Haimson, B., Cornet, F., 2003. ISRM suggested methods for rock stress estimation part 3: hydraulic fracturing (HF) and/or hydraulic testing of pre-existing fractures (HTPF). Int. J. Rock Mech. Min. Sci. 40, 1011–1020.

Han, Z., Wang, Chuanying, Wang, Chao, Zou, X., Jiao, Y., Hu, S., 2020. A proposed method for determining in-situ stress from borehole breakout based on borehole stereo-pair imaging technique. Int. J. Rock Mech. Min. Sci. 127, 104215.

He, M., Xia, H., Jia, X., Gong, W., Zhao, F., Liang, K., 2012. Studies on classification, criteria and control of rockbursts. J. Rock Mech. Geotech. Eng. 4, 97–114.

Hoberock, L.L., Bratcher, G.J., 1996. A new approach for determining In-Situ rock strength while drilling. J. Energy Resour. Technol. 118, 249–255.

Hoek, E., Brown, E.T., 2019. The Hoek–Brown failure criterion and GSI – 2018 edition. J. Rock Mech. Geotech. Eng. 11, 445–463.

Hudson, J.A., Harrison, J.P., 1997. In situ stress. In: Hudson, J.A., Harrison, J.P. (Eds.), Engineering Rock Mechanics. Pergamon, Oxford, pp. 41–69.

Ishida, T., Saito, T., 1995. Observation of core discing and in situ stress measurements; stress criteria causing core discing. Rock Mech. Rock Eng. 28, 167–182.

Li, H., He, M., Xiao, Y., Liu, D., Hu, J., Cheng, T., 2025. Granite strainbursts induced by true triaxial transient unloading at different stress levels: insights from excess energy ΔE. J. Rock Mech. Geotech. Eng. https://doi.org/10.1016/j.jrmge.2025.01.020.

Li, P., Liu, Y., Cai, M., Miao, S., Li, Y., Hu, Y., Gorjian, M., 2025. The overcoring technique for precise measurement of in situ rock stress at great depths: challenges and solutions. Engineering 46, 9–15.

Li, X., Chen, J., Ma, C., Huang, L., Li, C., Zhang, J., Zhao, Y., 2022. A novel in-situ stress measurement method incorporating non-oriented core ground re-orientation and acoustic emission: a case study of a deep borehole. Int. J. Rock Mech. Min. 152, 105079.

Li, Y., Peng, J., Zhang, P., Huang, C., 2021. Hard rock fragmentation in percussion drilling considering confining pressure: insights from an experimental study. Int. J. Rock. Mech. Min. 148, 104961.

Lin, H., Kang, W.H., Oh, J., Canbulat, I., Hebblewhite, B., 2020. Numerical simulation on borehole breakout and borehole size effect using discrete element method. Int. J. Min. Sci 30, 623–633.

Liu, K., Zou, C., Zhao, J., 2024. Dynamic tensile behaviour of rocks under confining pressure and high-rate loadings. Earth Energy Sci 1 (1), 1–13.

Liu, W., Deng, H., Zhu, X., Li, R., He, C., 2023. Experimental study of the rock cutting mechanism with PDC cutter under confining pressure condition. Rock Mech. Rock Eng. 56, 7377–7396.

Long, S., Yue, Z., Yue, W.V., Hu, H., Feng, Y., Yan, Y., Xie, X., 2025. Identification of rock layer interface characteristics using drilling parameters. Rock Mech. Rock Eng. 58, 1071–1098.

Ma, D., Wu, Y., Geng, H., Ma, X., Zhang, Y., Pu, H., Li, L., 2024. Mechanical behavior of multi-fracturing under confining pressure: effects of borehole diameter and rock type. Rock Mech. Rock Eng. 57, 11333–11350.

Ma, L., Ma, Z., Yu, H., Li, S., Pang, M., Wang, Z., 2022. Experimental investigation of thrust force in the drilling of titanium alloy using different machining techniques. Metals 12.

Mckenney, A.M., Corkum, A.G., 2020. Experimental evaluation of rapid flat jack testing with various shaped saw-cut slots. Rock Mech. Rock Eng. 53, 455–466.

Neuner, M., Abrari Vajari, S., Arunachala, P.K., Linder, C., 2023. A better understanding of the mechanics of borehole breakout utilizing a finite strain gradient-enhanced micropolar continuum model. Comput. Geotech. 153, 105064.

Ramsey, J.M., Chester, F.M., 2004. Hybrid fracture and the transition from extension fracture to shear fracture. Nature 428, 63–66.

Rao, K.U.M., Bhatnagar, A., Misra, B., 2002. Laboratory investigations on rotary diamond drilling. Geotech. Geol. Eng. 20, 1–16.

Ru, M., Lei, X.Q., Liu, X.M., Wei, Y.J., 2022. An equal-biaxial test device for large deformation in cruciform specimens. Exp. Mech. 62, 677–683.

Sakız, U., Aydın, H., Yaralı, O., 2021. Investigation of the rock drilling performance of rotary core drilling. Bull. Eng. Geol. Environ. 81, 24.

Seto, M., Utagawa, M., Katsuyama, K., Nag, D.K., Vutukuri, V.S., 1997. In situ stress determination by acoustic emission technique. Int. J. Rock Mech. Min. Sci. 34, 281.e1–281.e16.

Sjöberg, J., Christiansson, R., Hudson, J.A., 2003. ISRM suggested methods for rock stress estimation—Part 2: overcoring methods. Int. J. Rock Mech. Min. Sci, Special Issue of the IJRMMS: Rock Stress Estimation ISRM Suggested Methods and Associated Supporting Papers 40, 999–1010.

Tang, H., Liang, D.-C., Wu, Z.-J., Cheng, X., 2023. Energy analysis of intact granite based on test while drilling under different confining stresses and drilling parameters. Front. Earth Sci. 10.

Teale, R., 1965. The concept of specific energy in rock drilling. Int. J. Rock Mech. Min. Geom. Abs. 2, 57–73. https://doi.org/10.1016/0148-9062(65)90022-7.
Wang, X., Peng, P., Shan, Z., Yue, Z., 2022. In situ strength profiles along two adjacent vertical drillholes from digitalization of hydraulic rotary drilling. J. Rock Mech. Geotech. Eng. 15.
Wang, X.F., Zhang, M.S., Yue, Z.Q., 2021. In-situ digital profiling of soil to rock strength from drilling process monitoring of 200 m deep drillhole in loess ground. Int. J. Rock Mech. Min. 142, 104739.
Wu, S., Qiu, M., Yang, Z., Ji, F., Yue, Z., 2024a. Rapid profiling rock mass quality underneath tunnel face for Sichuan-Xizang railway. Undergr. Space 19, 138–152.
Wu, S., Yue, W.V., Qiu, M., Yue, Z., 2024b. Profiling of weathered argillaceous limestone rock with MWD data from advanced drilling for tunnelling along Wu-Kai expressway in Chongqing, China. Tunn. Undergr. Space Tech. 147, 105719.
Wu, S.Y., Yue, W.V., Yue, Z.Q., 2025. On drilling speed of London clay from MWD data with time-series algorithm for ground characterisation. Geotechnique 75, 166–179.
Yaşar, E., Ranjith, P.G., Viete, D.R., 2011. An experimental investigation into the drilling and physico-mechanical properties of a rock-like brittle material. J. Petrol. Sci. Eng. 76, 185–193.
Yu, B., Zhang, K., Niu, G., Xue, X., 2021. Real-time rock strength determination based on rock drillability index and drilling specific energy: an experimental study. Bull. Eng. Geol. Environ. 80, 3589–3603.
Yue, W.V., Wu, S., He, M., Qiao, Y., Yue, Z.Q., 2024. Digital monitoring of rotary-percussive drilling with down-the-hole hammer for profiling weathered granitic ground. J. Rock Mech. Geotech. 16, 1615–1636.
Yue, W.V., Yue, Z., Wu, W., Long, S., Qiao, Y., He, M., Zhu, H., 2025. Accurate determination of drilling parameters in time series for estimate of rock strengths. J. Rock Mech. Geotech. https://doi.org/10.1016/j.jrmge.2024.11.005.
Yue, X., Yue, Z., Yan, Y., Gao, D., Li, Y., 2023. Sensitivity analysis and rock strength prediction study of rotary drilling with drilling parameters. Geoenergy Sci. Eng. 230, 212169.
Yue, Z.Q., Lee, C.F., Law, K.T., Tham, L.G., 2004. Automatic monitoring of rotary-percussive drilling for ground Characterization—Illustrated by a case example in Hong Kong. Int. J. Rock Mech. Min. 41, 573–612.
Zhao, R., Yao, R., Zhang, T., Shi, S., 2024. Estimation of tunnel in-situ stress magnitude and direction using measurement while drilling data and Acoustic wave information. Tunn. Undergr. Space Technol. 152, 105905.
Zhao, T., Qin, Q., 2023. Characterization methods for current in-situ stress in oil and gas reservoirs: a mini review. Front. Earth Sci. 11.
Zou, X., Song, H., Wang, C., 2021. A high-precision digital panoramic borehole camera system for the precise analysis of in situ rock structures. Rock Mech. Rock Eng. 54, 5945–5952.

Wendal Victor Yue is currently a PhD student under the supervision of Prof. Manchao He and Prof. Hehua Zhu in Department of Civil Engineering from Tongji University, China. He received his BSc and MSc from University of Alberta and University of Toronto, Canada, respectively. His research focuses on drilling process monitoring (DPM) for analysing drilling mechanism to characterize the properties of rock and soil.